Journal of Drug Delivery Science and Technology 87 (2023) 104811

Contents lists available at ScienceDirect

Journal of Drug Delivery Science and Technology

journal homepage: www.elsevier.com/locate/jddst

Nanostructured lipid carrier for the ophthalmic delivery of haloperidol metabolite II valproate ester (±)-MRJF22: A potential strategy in the treatment of uveal melanoma

Cinzia Cimino [a,b,c], Claudia Giovanna Leotta [d], Agostino Marrazzo [c,e], Teresa Musumeci [b,c], Giovanni Mario Pitari [d], Rosario Pignatello [b,c], Angela Bonaccorso [b,c], Emanuele Amata [e], Carla Barbaraci [e,1], Claudia Carbone [b,c,*]

[a] PhD in Biotechnology, Department of Biomedical and Biotechnological Sciences, University of Catania, Via Santa Sofia 97, 95123, Catania, Italy
[b] Laboratory of Drug Delivery Technology, Department of Drug and Health Sciences, University of Catania, Viale A. Doria 6, 95124, Catania, Italy
[c] NANOMED, Research Centre for Nanomedicine and Pharmaceutical Nanotechnology, University of Catania, Italy
[d] Vera Salus Ricerca S.r.l., Via Sigmund Freud 62/B, 96100, Siracusa, Italy
[e] Medicinal Chemistry Laboratory, Department of Drug and Health Sciences, University of Catania, Viale A. Doria 6, 95124, Catania, Italy

ARTICLE INFO

Keywords:
NLC
Ophthalmic delivery
DSC
Stability
Mucoadhesion
Cell proliferation

ABSTRACT

Among the eye tumors, uveal melanoma is one of the most diffuse and aggressive, affecting mainly the choroid, but also the ciliary body and the iris. Promising pharmaceutical therapies involve histone deacetylase inhibitors and sigma-ligands: these targets were combined in a new-synthetized prodrug, namely (±)-MRJF22, which demonstrated to perform antiangiogenic activity, as well as its (*R*)- and (*S*)-enantiomers. Since this cancer mainly occurs in the posterior segment of the eye, the therapeutical use of this prodrug is limited by the presence of ocular barriers. Herein, lipid nanoparticles were selected for their potential ophthalmic application to encapsulate (±)-MRJF22 prodrug and its (*R*)- and (*S*)-enantiomers. The prepared nanoparticles demonstrated to be suitable for the intended ophthalmic administration in terms of size, homogeneity, zeta potential, pH and osmolality. DSC and FTIR analyses were performed on the formulations, and their long-term stability was confirmed by accelerated stability studies. Mucoadhesive studies suggested a potential good interaction with ocular surface epithelia, thus enhancing the ocular residence time of the formulations. *In vitro* release studies demonstrated a sustained and prolonged release of the prodrugs loaded in the colloidal suspensions. Cytocompatibility and proliferation assays were performed on uveal melanoma 92-1 cell line, confirming the suitability of the formulations and their potential application in the treatment of uveal melanoma.

1. Introduction

Uveal melanoma (UM) is one the most aggressive malignant tumor of the eye, and the most diffused primary intraocular cancer among adults [1]; the annual incidence is 0.24 per million among Blacks, 0.9 among Hispanics and 6.3 among Whites, with a prevalence for men, who develop bigger tumors. UM occurs in choroid for about 90%, in the ciliary body for 7% and in the iris for 3% [2]. One of the earliest symptoms is blurred vision, but it could be diagnosed also in asymptomatic patients through routine controls. Predisposing factors resulted to be ability to tan, hair color and skin color, BRCA1-associated protein 1 mutation, oculodermal or ocular melanocytosis, choroidal or cutaneous or iris nevus [1,3,4]. The main criticism associated with this tumor is the great tendency to metastasize: the involved organs are liver (90% of cases), lungs and soft tissues, where metastases generally occur in 5 years for 25% of patients and in 10 years for 34%, since the first tumoral occurrence [5]. The mortality rate is also quite high (80% in one year and 92% in two years [6]) and is related to liver compromission.

Nowadays, the most successful approaches involve surgery, radiotherapy and also enucleation for larger melanomas. As pharmaceutical

* Corresponding author. Department of Drug and Health Sciences, University of Catania, Viale A. Doria 6, 95125, Italy.
E-mail address: claudia.carbone@unict.it (C. Carbone).
[1] Present address: Laboratory of Medicinal Chemistry (CSIC Associated Unit), Faculty of Pharmacy and Food Sciences, and Institute of Biomedicine (IBUB), University of Barcelona, Av. Joan XXIII, 27-31, 08028 Barcelona, Spain.

https://doi.org/10.1016/j.jddst.2023.104811
Received 3 April 2023; Received in revised form 26 July 2023; Accepted 2 August 2023
Available online 4 August 2023
1773-2247/© 2023 The Authors. Published by Elsevier B.V. This is an open access article under the CC BY license (http://creativecommons.org/licenses/by/4.0/).

treatments to contrast UM, inhibitors of histone deacetylase (HDACi) could be used, since this enzyme is responsible of the increase of the transcription gene involved in cell growth, resulting in cell cycle advancement and DNA duplication: the inhibition of histone deacetylase (HDAC), using HDACi as valproic acid, induces the death of cancer cells thus reducing tumor development both *in vivo* and *in vitro* [7]. Moreover, sigma receptors are also targeted in the treatment of UM for their role in cell proliferation and survival: in particular, σ_1 increases the secretion of vascular endothelial growth factor (VEGF) and encourages motility [8,9], while σ_2 promotes autophagy and apoptosis [10]. Recently, a new synthetized drug was developed combining valproic acid histone deacetylase inhibition and haloperidol metabolite II (HP-mII) antagonism for σ_1 and agonism for σ_2, resulting in a prodrug, (±)-MRJF22 and its enantiomers, with a great potential in the treatment of UM, as emerged from *in vitro* studies which ascertained its antiangiogenic activity on Human Retinal Endothelial Cells (HREC) [9].

Pharmacological treatments find well-known impediments related to the location of the tumor in the posterior chamber of the eye: the presence of numerous physiological barriers strongly limits the bioavailability of the drug to the active site (lower than 3–5% of the administered dose). In order to overcome these limits, drug delivery systems represent a promising strategy to reach the inner tissues of the eye, guaranteeing prolonged and sustained release, capability to achieve the target site and longer permanence which enhance corneal permeation [11].

Among the various platforms that have been proposed to achieve the inner eye, nanostructured lipid carrier (NLC) resulted to be very advantageous due to their ability to encapsulate great amount of encapsulated lipophilic drug, their high stability, the ability to perform controlled release, their efficiency in ocular delivery [12,13].

Basing on these considerations, this work aimed to the encapsulation of (±)-MRJF22 enantiomers into NLC, intended for ophthalmic application in the treatment of UM. Racemic mixture and both (*R*)- and (*S*)-enantiomers, preliminarily characterized by Differential Scanning Calorimetry (DSC), were successfully encapsulated into nanoparticulate systems using phase inversion temperature technique (PIT method), thus obtaining (*M*)-NLC, (*R*)-NLC and (*S*)-NLC, respectively. NLC were prepared using surfactant and lipids previously demonstrated to be safe on Statens Seruminstitut Rabbit Cornea (SIRC) cell line for the ophthalmic drug delivery [14]. Nanosuspensions were characterized from physico-chemical and technological points of view, measuring pH, osmolality, but also mean particles size (Z-ave), polydispersity index (PDI) and zeta potential (ZP) through Photon Correlation Spectroscopy (PCS) analysis. Accelerated stability studies in constant climate chamber were also performed following ICH guidelines Q1A (R2), storing the samples for 6 months at 40 ± 2 °C and 75 ± 5% RH. The produced NLC were characterized through DSC analysis and Fourier-transform infrared (FTIR) spectroscopy. Preliminary mucoadhesive evaluation of NLC in simulated tear fluid (STF) was performed up to 4 h to assess their potential interaction with mucin, one of the main glycoproteins present in the mucus layer adjacent to ocular surface epithelia. Encapsulation efficiency (EE%) of the prodrug into NLC was measured and *in vitro* release studies were performed using Franz-type diffusion cells. Biological studies were performed *in vitro* on human uveal melanoma (UM) 92-1 cells to evaluate NLC safety and antiproliferative activity of enantiomer-loaded NLC.

2. Materials and methods

2.1. Materials

Kolliphor RH40 was provided by BASF Italia S.p.a. (Cesano Modena, Italy); Oleoyl Macrogol-6 Glycerides (Labrafil) was a gift from Gattefossé Italia s.r.l. (Milano, Italy); Hydrogenated Coco-Glycerides (Softisan 100) was bought from IOI Oleo GmbH (Oleochemicals, IOI group); Isopropyl myristate (IPM) was purchased from Farmalabor (Canosa di Puglia, Italy); Tris (hydroxymethyl)aminomethane buffer was bought from Merck (Darmstadt, Germany). (±)-MRJF22, (*R*)-(+)-MRJF22 and (*S*)-(−)-MRJF22 were synthetized by the research group of Prof. Marrazzo, in the Medicinal Chemistry Laboratory of the Department of Drug and Health Sciences (University of Catania) [9]. Mucin (mucin from porcine stomach type II), NaCl, $NaHCO_3$, $CaCl_2{\cdot}2H_2O$ and KCl were purchased from Sigma-Aldrich S.r.l. (Milan, Italy). Regenerated cellulose membranes (Spectra/Por CE; Mol. Wet. Cutoff 3500) were supplied by Spectrum (Los Angeles, CA, USA). Human UM 92-1 cell line was purchased from the Cell Factory-IST (Genova, Italy). Media and reagents RPMI-1640 medium, fetal bovine serum (FBS), L-glutamine, penicillin and streptomycin used for cell studies were from Euroclone S.p.A. (Pero, Milan, Italy). All solvents (LC grade) were from VWR International (Milan, Italy).

2.2. Preliminary studies on free prodrugs

2.2.1. Differential Scanning Calorimetry on free prodrugs

On a Mettler DSC 12E equipped with a Haake thermocryostat type D8-G, DSC scans of the three compounds were executed. Data were collected using a Mettler TA89E and FP89 system software and the instrument was calibrated using indium. The control pan was left empty. Each sample was scanned at a rate of 5 °C/min for heating and 10 °C/min for cooling in the temperature range of 10–200 °C.

2.2.2. Stability at PIT method's temperature

Prodrugs were diluted in a methanol-0.5% diethylamine mixture and put on a heating plate (68 ± 2 °C) for 5 min, corresponding to the time-exposure to heating of the lipid phase of NLC where the drugs had been solubilized, thus undergoing the heat treatment required by PIT technique. The prodrugs' solutions were then examined through UV–vis spectrophotometer (UH5300 UV–Visible Double-Beam Spectrophotometer, Hitachi Europe, Milan, Italy) and compared to the respective reference spectra.

2.3. Nanoparticle production

NLC were prepared using the PIT technique [15]. The lipid mixture (Softisan:IPM at a 2:5 wt ratio) was added with the surfactant mixture (7% w/V) [16]. The prodrugs (0.02% w/v) were added to the lipid phase. The aqueous phase consisted of TRIS buffer (pH 7.4). Both phases were heated at 68 ± 2 °C. Then, the aqueous phase was dropped into the lipid phase, leading to the formation of blank NLC or loaded formulations (*M*)-NLC, (*R*)-NLC and (*S*)-NLC, encapsulating (±)-MRJF22, (*R*)-(+)- MRJF22 and (*S*)-(−)-MRJF22, respectively. After mixing on a magnetic plate at room temperature, the samples were vortexed (Heidolph Rea×2000, VWR, Milan, Italy), then kept in the freezer for 15 min and stored at 4 °C.

Each formulation was centrifuged at 13.000 rpm for 90 min at 4 °C using an ultracentrifuge (SL16R Centrifuge, Thermo Scientific, Rodano, Italy) fitted with a fixed body rotator, in order to remove the excess of surfactants and the amount of prodrugs that remained non-encapsulated in the colloidal suspensions.

2.4. Physical-chemical and technological characterization of NLC

2.4.1. Osmolality and pH

An osmometer (Osmomat 3000, Gonotec, Berlin, Germany) was used to assess the osmolality of the samples, which was previously calibrated using ultra-purified water and physiological solution. The pH values of the samples were determined using a pH meter (Mettler Toledo, Milano, Italy), calibrated using solution with defined pH 4.0, 7.0 and 10.0.

2.4.2. Photon Correlation Spectroscopy (PCS)

The produced NLC were characterized by Photon Correlation Spectroscopy (PCS) using a Zetasizer Nano S90 (Malvern Instruments,

Malvern, UK), to evaluate mean particle size (Z-ave), polydispersity index (PDI) and zeta potential (ZP). Samples analyses were performed in triplicate after 1:20 dilution with ultra-purified water.

2.4.3. Encapsulation efficiency

The effective amount of the encapsulated prodrug in the lipid matrix of NLC was indirectly evaluated measuring the amount of prodrug not encapsulated. Each formulation was centrifuged at 13.000 rpm for 90 min at 4 °C. The obtained supernatants, separated from the resulting pellet, were diluted in methanol-0.5% diethylamine mixture (1:5 v/v) and centrifuged at 13.000 rpm for 30 min at 4 °C. The supernatants were analyzed using a UV–vis spectrophotometer. The encapsulation efficiency (EE %) was calculated using the following equation:

EE% = amount of prodrug entrapped/total amount of prodrug used × 100.

2.4.4. Accelerated stability studies

Accelerated stability studies of blank and loaded formulations were conducted as described in ICH guidelines Q1A (R2) by incubating the prepared formulations at accelerated conditions (40 ± 2 °C temperature and 75 ± 5% RH) for 6 months in constant climatic chamber (BINDER GmbH, KBF-S 115 E6, Tuttlingen, Germany). The stability was measured in terms of mean particle size and PDI. The effect of temperature and humidity was observed at specific time-points: 0, 1, 2, 3, 4, 5, and 6 months.

2.4.5. Dynamic scanning calorimetry

In order to investigate the influence of the preparation method on the selected prodrug-loaded NLC, DSC was performed on NLC, (*M*)-NLC, (*R*)-NLC, (*S*)-NLC and on raw materials – such as Kolliphor and Softisan – with the equipment described in Paragraph 2.2.1. The control pan was left empty. Each sample was scanned at a rate of 5 °C/min for heating and 10 °C/min for cooling in the temperature range of 10–130 °C.

2.4.6. Fourier-transform infrared (FTIR) spectroscopy

The IR spectra of nanoparticles raw materials, prodrugs and NLC formulations were recorded in KBr disks, after solubilization in dichloromethane, on a FTIR spectrometer (PerkinElmer Spectrum RX I, Waltham, MA, USA) equipped with a diamond window and a zinc selenide crystal (diamond/ZnSe) and an attenuated total reflectance (ATR) accessory.

2.4.7. Mucoadhesive studies

Two different *in vitro* methods were performed in order to assess the mucoadhesive properties of NLC after incubation with mucin in simulated tear fluid (STF). Briefly, mucin (0.1% w/v) was suspended in STF (NaCl 0.68 g, $NaHCO_3$ 0.22 g, $CaCl_2{\cdot}2H_2O$ 0.008 g, KCl 0.14 g, and distilled deionized water to 100 mL) and stirred overnight to allow its complete dispersion. The interaction between each NLC and mucin was determined by mixing mucin dispersion and NLC (1:1 v/v) for 15 min at 25 °C and after incubation at 37 °C up to 4 h by turbidimetric assay and mucin particle method. In particular, turbidimetric measurements were evaluated comparing the absorbances at 650 nm by UV–vis spectrophotometer of the native mucin and each NLC-mucin dispersion after 0, 1, 2, 3 and 4 h of incubation. Mucin particle method was performed by measuring the change in NLC particles size and zeta potential after incubation with mucin at the same time points, to estimate the extent of their mucoadhesive property.

2.4.8. In vitro drug release

Franz-type diffusion cells (LGA, Berkeley, CA, USA) were used to assess molecules' release profiles from free prodrugs solutions and from prodrug-loaded NLC formulations. Before being installed in Franz cells, 0.75 cm^2 of regenerated cellulose membranes (Spectra/Por CE; Mol. Weight Cut-off 3.5 kDa) were moistened for 24 h in the same medium used in the receptor compartment (4.5 mL), which was a 50:50 v/v combination of tris(hydroxymethyl)aminomethane buffer (TRIS pH 7.4) and methanol-0.5% diethylamine, thermoset at 35 °C and stirred at 600 rpm. The donor compartments were then filled with 500 μL of each sample's pellet. At planned time intervals (from T = 0–24 h), 500 μL of receptor medium was withdrawn and replaced with an equivalent volume of medium equilibrated to 35 °C to guarantee pseudo-sink conditions. To evaluate the drug content, each sample was twofold diluted with medium and examined using a UV–vis spectrophotometer. Racemic mixture released from (*M*)-NLC was analyzed at both the absorption wavelengths typical of the enantiomers (λ 222.0 nm for the (*S*)-enantiomer and λ 224.0 nm for the (*R*)-enantiomer), and the mean release value was calculated.

2.5. In vitro cell studies

2.5.1. Cell cultures

Human UM 92-1 cells were maintained at 37 °C (5% CO_2) in RPMI-1640 medium, containing 10% fetal bovine serum (FBS), 2 mM L-glutamine, 100 units/mL penicillin and 100 μg/mL streptomycin. Cells were split when subconfluent (70–80% confluence) and investigated within passages 2-15.

2.5.2. Cytotoxicity and cell proliferation

Cytotoxicity was assessed in confluent UM 92-1 cell monolayers treated for 24 h with the indicated chemicals. For cell proliferation, 92-1 cells (2.6×10^3) were seeded in 96-well plates and grown at optimum culture conditions for 72 h (at a confluence of ~60%). Then, cells were treated with the indicated compounds for additional 48 h. For both assays, at the end of treatments cells were fixed (in 4% paraformaldehyde) and stained with crystal violet solution (1% aqueous solution). Crystal violet staining was evaluated by measuring the absorbance at 590 nm, after crystal violet extraction with 10% acetic acid (at room temperature for 10 min), with a microplate reader (Synergy HT, Agilent BioTek, Santa Clara, CA).

2.6. Statistics

Statistical analysis for physical-chemical and technological characterization was performed by Student's t-test. For mucoadhesive studies, two-way ANOVA was performed; multiple comparisons were performed according to Tukey's multiple comparisons test for the turbidimetric assay, and for particle mean size and ZP data. For biological studies, results are shown as mean ± SD of three independent experiments performed in quadruplicate; statistical comparisons were performed by unpaired Student's t-test; all analyses were done with GraphPad Prism 8 or 9.3.1 (GraphPad Software, Inc., San Diego, CA, USA). P values were considered significant at $\alpha \leq 0.05$.

3. Results and discussion

3.1. Preliminary studies on free prodrugs

In order to assess the thermal behaviour of racemic mixture and enantiomers, DSC analysis was performed.

As it is possible to observe in Fig. 1, the racemic mixture (±)-MRJF22 (blue line) showed the presence of a single well-defined peak, with a melting point of about 80 °C. This behaviour is characteristic of a species which forms racemic solid solutions. The (*S*)-(−)-MRJF22 thermogram resulted to be composed of an asymmetric peak with the main transition at 82 °C while the curve obtained for (*R*)-(+)-MRJF22 showed the presence of main transition at 84 °C with a little enlargement of the curve. The second peak highlighted in (*S*)-(−)-MRJF22 profile at 78 °C, could be related to the presence of a residuum from the synthetic process. Moreover, the presence of the melting point could relate to the possibility that molecules exist in amorphous state. The difference in melting point values for the tested molecules is not relevant and could be

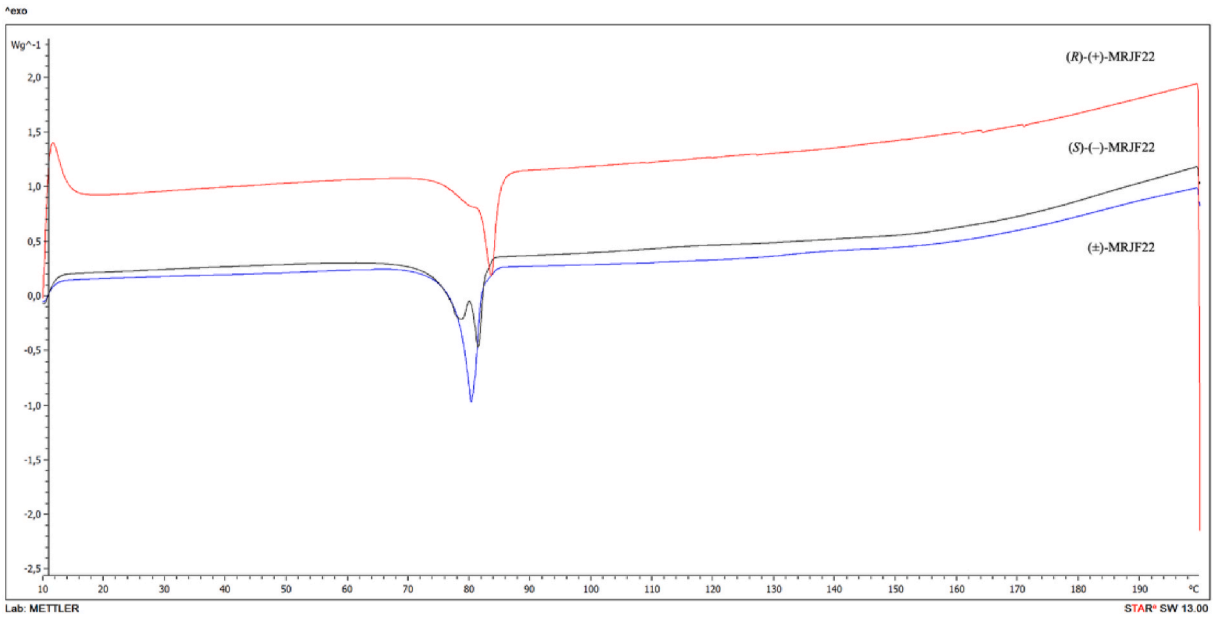

Fig. 1. DSC thermograms of (*R*)-(+)-MRJF22 (red line), (*S*)-(−)-MRJF22 (black line) and (±)-MRJF22 (blue line). (For interpretation of the references to color in this figure legend, the reader is referred to the Web version of this article.)

correlated to same thermotropic stability [17].

DSC results also suggested the suitability of the PIT method for loading the prodrugs into NLC, since the operation temperature – which is lower than the melting points of the compounds – avoids the occurrence of molecule degradation.

To further confirm the suitability of the PIT method, thermal stability studies were performed by heating the compounds solutions at 68 ± 2 °C and analyzing by UV–vis spectrophotometry. This method was already used by Rizzo and coworkers [18], who found that the formation of degradation compounds or intermediates could affect the UV value obtained at the selected wavelength. Thus, the spectra obtained after heating were compared with the ones of reference compounds' solutions (data not reported). For both enantiomers it emerged no difference in absorbance at respective characteristic peaks' wavelengths, thus confirming the stability of the prodrugs at the operative temperatures; on the other hand, a slight decrease in racemic mixture absorbance was highlighted, suggesting a possible lower stability of the compound at the operating temperature of PIT technique. The assessment of the suitability of the operative temperatures allowed to proceed with the encapsulation of prodrug into NLC using the selected organic solvent free and eco-friendly lab-scale technique [19], that has been previously reported to produce stable colloidal systems [20].

3.2. Physico-chemical and technological characterization of NLC

Raw materials for nanoparticle preparation were chosen properly to be biocompatible for ocular administration, thus allowing the interactions with cell membranes and avoiding side effects [21]. Kolliphor and Labrafil were selected as components of the surfactant mixture basing on previous studies [22], since they demonstrated to produce particles with adequate mean diameter and homogeneity, able to guarantee optimal *in vitro* release profiles. Furthermore, their biocompatibility at the ocular site was already demonstrated by our research group [14]. Surfactants and lipids amounts were evaluated considering previous findings [16] aiming to reduce surfactant percentage – for tolerability reasons – while assuring adequate characteristics in terms of particle size.

Considering the intended ocular administration route, pH and osmolality values have to be modulated in order to fall within the ocular tolerated ranges. In particular, pH values lower than 4 or higher than 10 induce chemical damage to the eye [23], while values close to the physiological pH (7.11 ± 1.5) are well-tolerated [24]. European Pharmacopoeia and FDA both require a pH between 6.8 and 7.4 for liquid preparations used for the ocular site [25] (https://www.fda.gov/media/111063/download accessed on 25th July 2023). Regarding osmolality, this parameter has to be carefully modulated in order to provide a safe passage of particles through biological membranes; specifically, the optimal range is the tears one, between 280 and 300 mOsm/Kg [14], even though the eye is able to tolerate values from 200 to 500 mOsm/Kg (https://www.fda.gov/media/111063/download accessed on 25th July 2023). Aiming to obtain a good tolerability, TRIS buffer was selected as the aqueous phase of the colloidal system. Consequently, the prepared samples showed similar pH and osmolality values (Table 1), falling within the range required for ophthalmic administration route, thus suggesting a good cellular tolerability, which was further investigated.

As extensively reported in literature, nanoparticle size has an important influence on many parameters, such as target tolerability, formulation stability, drug distribution, residence time at the administration site. Considering ophthalmic administration, generally particles with diameter of 100 nm are actively complement receptor-mediated phagocytized in the pathway between cornea and conjunctiva, while particles in the 200–300 nm range are transported into the corneal structure through intracellular routes [26,27]. Apart for the absorption

Table 1
Physical-chemical and technological characterization of NLC, (*M*)-NLC, (*S*)-NLC and (*R*)-NLC. pH, osmolality, mean particle size (Z-ave), PDI, zeta potential (ZP), and encapsulation efficiency are reported, and each value is the mean of three measurements ± SD. *p < 0.025.

Sample	pH ± SD	Osm (mOsm/kg) ± SD	Z-ave (nm) ± S.D.	PDI ± SD	ZP (mV) ± SD	EE% ± SD
NLC	7.43 ± 0.12	0.257 ± 0.019	139.1 ± 9.693	0.229 ± 0.022	−5.63 ± 0.731	/
(*M*)-NLC	7.28 ± 0.02	0.228 ± 0.005	146.6 ± 10.38	0.264 ± 0.055	−4.13 ± 0.128*	87.55 ± 11.61
(*S*)-NLC	7.36 ± 0.06	0.255 ± 0.015	142.7 ± 5.383	0.241 ± 0.022	−6.84 ± 2.91	57.17 ± 2.29
(*R*)-NLC	7.36 ± 0.06	0.254 ± 0.017	150.8 ± 6.704	0.255 ± 0.017	−6.68 ± 2.49	68.72 ± 6.56

mechanism, particles smaller than 250 nm are required in order to be suitable for ophthalmic delivery [28] and a mean particle diameter lower than 200 nm is necessary in order to guarantee an adequate ocular permeation [29].

PCS analysis showed that the produced colloidal systems were composed of small and homogeneous particles, with a mean particle size lower than 150 nm and a polydispersity index (PDI) lower than 0.26 for all formulation, as confirmed by the single and narrow peak obtained for size distribution, with a slight increase after drug loading. According to literature, a slight increase in particle size after drug encapsulation was expected because of the accommodation space required by the active molecule into the nanoparticle [30] and due to changes in the interfacial tension or viscosity induced by the presence of the active molecule causing inefficient particle size reduction [31]. The addition of the prodrug did not significantly modify NLC Z-ave ($p < 0.025$). The optimal values of correlation coefficient (Supplementary Fig. 1), obtained for all measurements, confirmed the results of the analyses. We also evaluated the ZP, a parameter that describes the particles' surface charge, which is responsible of the physical stability of the colloidal system. The almost neutral ZP values which were obtained for all formulations suggest the possible occurrence of physical instability, since ZP values between −25 mV and 25 mV are not able to guarantee long term stability due to insufficient nanoparticles repulsion, causing potential aggregational phenomena [16]. On the other hand, mean particle dimensions obtained for all the samples suggest a possible prevention of thermodynamical instability caused by Ostwald ripening [32]. Considering these hypotheses, it resulted necessary to perform further evaluations of samples' physical stability. Accelerated stability studies were performed following the ICH guidelines Q1A (R2), by storing the samples for 6 months under the effect of high temperature and humidity, thus allowing the prediction of formulations' behavior at room temperature for 1 year [33]. At each time point (0, 1, 2, 3, 4, 5 and 6 months), Z-ave and PDI were measured and compared (Fig. 2). Data obtained from T0 analysis were considered the referring values for the *t*-test statistical analysis.

As highlighted in Fig. 2, all NLC showed a good physical long-term stability. This result could be attributable to the presence of the mixture of surfactant and co-surfactant, which provides a high stabilization of particles' surface [34]. In particular, (*S*)-NLC was the most stable sample, with particle size remaining almost unchanged during the whole storage time and showing only one significant variation in particle size after 2 months, with the lower tabulated t-value ($p < 0.0025$). Similarly, (*M*)-NLC was stable with significant variation ($p < 0.005$) in particle size after 4 and 5 months of storage at accelerated conditions, while (*R*)-NLC showed a significant variation ($p < 0.01$) in particle size at all analyzed time points. Even if a certain significant decrease in particle size was observed, all NLC maintained features adequate for the ophthalmic application, therefore these samples could be proposed for a storage at room temperature during industrial production and distribution.

In Table 1 it is also possible to observe encapsulation efficiency values (EE%), which resulted to be higher for the racemic mixture in (*M*)-NLC compared to enantiomers, with (*R*)-enantiomer having a 10% higher EE% compared to (*S*)-enantiomer, which could be attributed to a different arrangement of each prodrug with the other NLC components.

In Fig. 3 are reported the thermograms of unloaded and prodrug-loaded NLC. The lower melting temperatures and broader endothermic peaks presented by all NLC formulations indicated a less ordered crystalline structure compared to the single raw materials, as well described by values reported in Table 2. The absence of the peak related to prodrug in the loaded NLC demonstrated the successful incorporation of the molecules into the core of the nanoparticles [15,35].

FT-IR analysis was performed aiming to qualitatively identify the main functional groups of the materials (Supplementary Fig. 2) and NLC formulations, in order to highlight the occurrence of potential chemical interactions during nanoparticles' preparation, but also to assess the encapsulation of prodrugs into NLC [36].

Comparing the spectra of the loaded-NLC to the respective free prodrugs (Fig. 4-A,B,C), it is possible to highlight their successful encapsulation into the nanocarrier since some of the characteristic peaks of free molecules were not visible in loaded-NLC spectra, as the one at about 1650 cm^{-1} (C=C typical of conjugated alkene).

The spectra of blank NLC and loaded-NLC (Fig. 4-D) were very similar with the presence of characteristic peaks in all the obtained analysis. The peak at about 3440 cm^{-1} could be referrable at N–H stretching of I or II amines, that were present in the surfactant Kolliphor, or to O–H stretching of alcohols, typical of the co-surfactant Labrafil. The peak at about 2920 cm^{-1} is shown in all NLC formulations but also in the spectra of raw materials (Supplementary Fig. 2), being relatable to C–H stretching of alkanes (largely present in Labrafil, in the solid lipid Softisan and in the liquid lipid IPM) and to O–H stretching of intramolecular alcohols or of carboxylic acids (present in Labrafil). Peaks at about 1730 cm^{-1} were referrable to C=O stretching of esters, as in IPM structure. At lower wavelengths, in all the spectra was detected some noise, even if it is possible to identify peaks at about 1450 cm^{-1} attributable to C–H bending of alkane methyl groups (largely present in almost all the used materials) and at about 1100 cm^{-1} referrable to C–O stretching of aliphatic esters (of Labrafil and Kolliphor, as confirmed by their individual spectra in Supplementary Fig. 2), but also referrable to C–F stretching (Kolliphor).

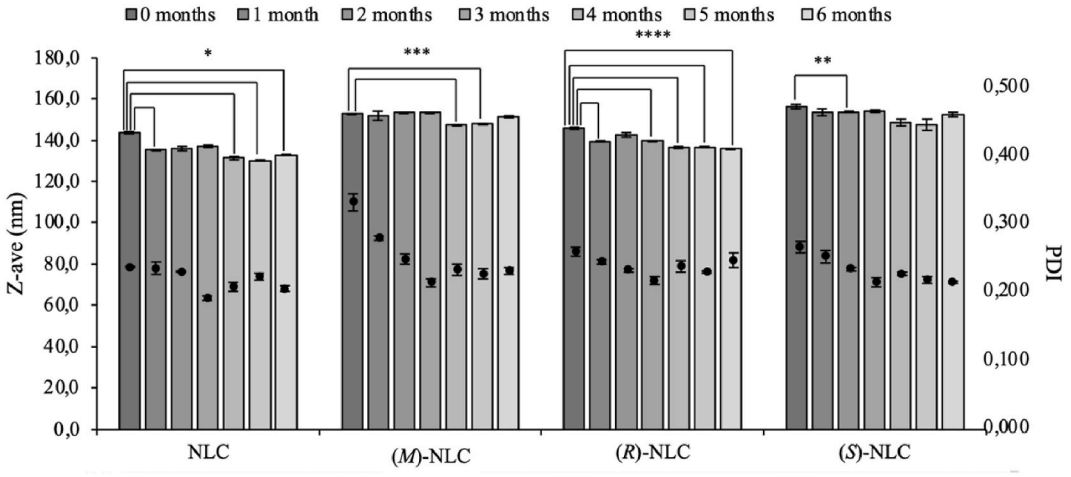

Fig. 2. Effect of accelerated (40 ± 2 °C and 75 ± 5% RH) storage conditions on mean particle size and PDI of NLC, (*M*)-NLC, (*R*)-NLC and (*S*)-NLC. Each value is the mean of three analysis ±SD. *$p < 0.001$; **$p < 0.0025$; ***$p < 0.005$; ****$p < 0.01$.

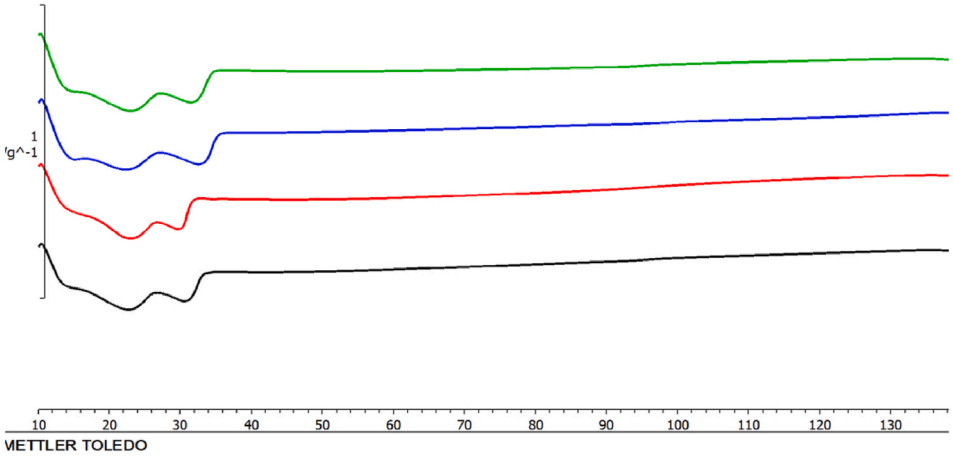

Fig. 3. Thermograms of NLC (black line), (*M*)-NLC (red line), (*R*)- NLC (blue line) and (*S*)-NLC (green line). (For interpretation of the references to color in this figure legend, the reader is referred to the Web version of this article.)

Table 2
Thermal properties of raw materials and of NLC, (*M*)-NLC, (*R*)-NLC and (*S*)-NLC.

	$T_{melting}$/°C (first peak)	$T_{melting}$/°C (second peak)	$T_{melting}$/°C (third peak)
Kolliphor RH40	31.07	34.4	
Softisan 100	32.34	38.72	
NLC	22.62	30.63	145.56
(*M*)-NLC	23.03	29.70	145.14
(*S*)-NLC	22.29	32.55	145.48
(*R*)-NLC	22.86	31.45	145.95

This qualitative FT-IR analysis confirmed the successful prodrugs encapsulation into nanoparticles; moreover, the absence of new peaks suggests that the interaction between prodrugs and excipients didn't produce new bonds, thus the active molecules were physically entrapped into the nanoparticles without modification of their main structure and potential activity [37].

In vitro release of (±)-MRJF22, (*R*)-(+)-MRJF22 and (*S*)-(−)-MRJF22 respectively from (*M*)-NLC, (*R*)-NLC and (*S*)-NLC was assessed using Franz-type diffusion cells (Fig. 5) and compared with free prodrug release.

As expected, all prodrugs' solutions (Fig. 5-A) showed an immediate release, with both enantiomers achieving 100% of drug released in 3 h, while racemic mixture was completely released in 5 h from the

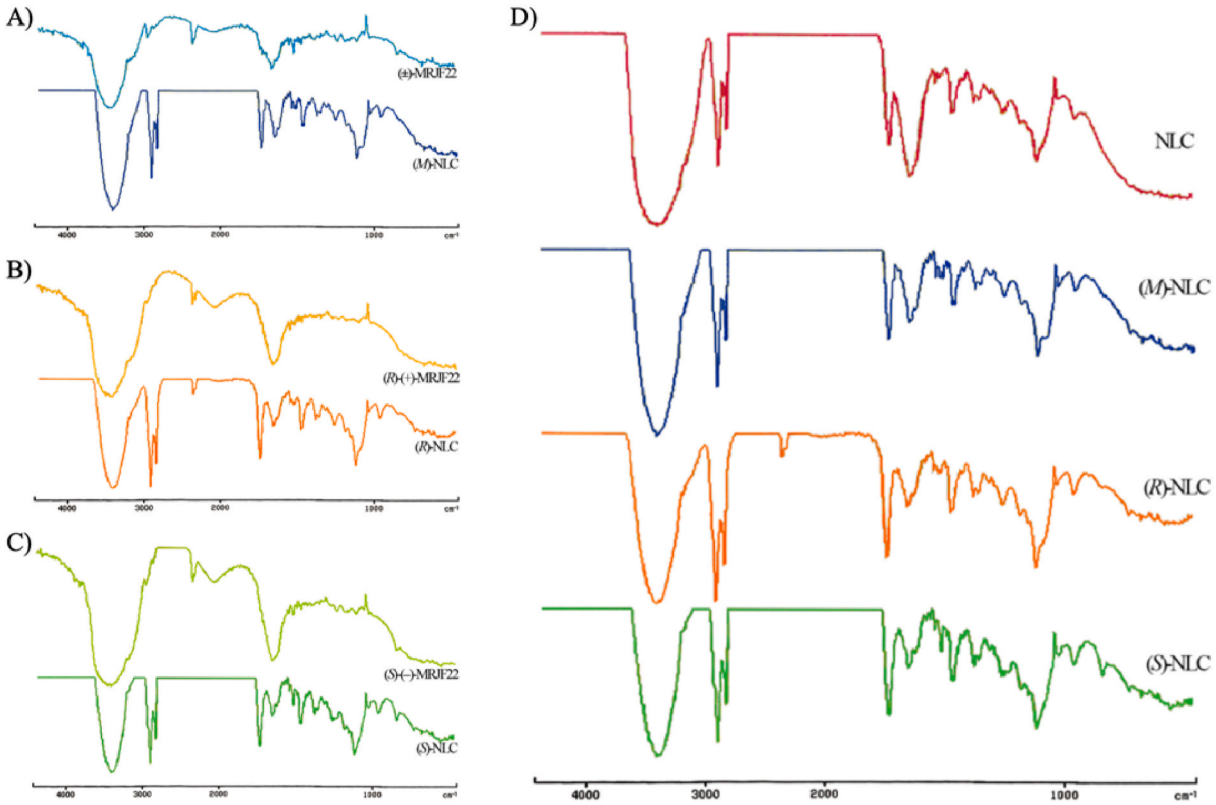

Fig. 4. FT-IR curves of (±)-MRJF22 and (*M*)-NLC (**A**); (*R*)-(+)-MRJF22 and (*R*)-NLC (**B**); (*S*)-(−)-MRJF22 and (*S*)-NLC (**C**); and comparison between all the produced nanosystems (**D**).

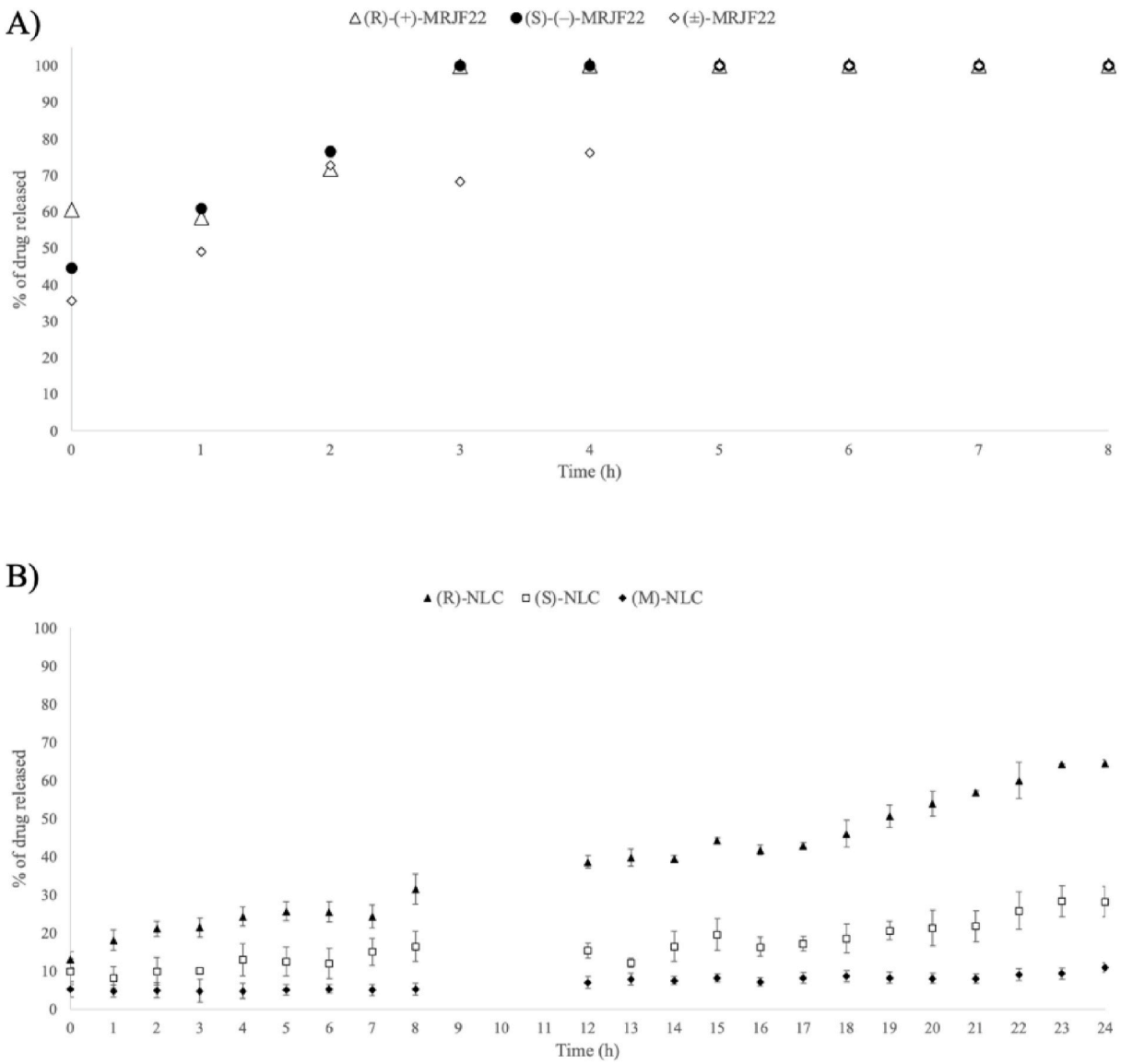

Fig. 5. *In vitro* release profiles of free prodrugs solutions (**A**) and prodrug-loaded NLC (**B**) in 50:50 mixture of tris(hydroxymethyl)aminomethane buffer (TRIS) and methanol-0.5% diethylamine at 35 °C. Each point represents the mean value of three different experiments ± S.D.

beginning of the experiment. As aimed, release profiles of loaded-NLC (Fig. 5-B) were very different compared to prodrugs' solutions, showing a slow and prolonged release for 24 h. In particular, (*M*)-NLC showed an initial 5% of drug released, which remained basically unchanged throughout the experiment, despite racemic mixture showed the highest EE% (87.55%) among the loaded-NLC. On the other hand, (*S*)-NLC showed an initial 10% of active molecule immediately released, reaching less than 30% at 24 h. Similarly, (*R*)-NLC showed a 13% of prodrug released at T0, followed by a sustained release which reached almost 65% after 24 h from the beginning of the experiment. It is interesting to note that the release behaviours of the two enantiomers are analogue, but with a higher amplitude of (*R*)-enantiomer compared to (*S*)-enantiomer. The different release at 24 h could be referred to the different EE% values measured for (*R*)-NLC and (*S*)-NLC, which were respectively 68.72% and 57.17% and to a different accommodation of the prodrugs into the lipid matrix.

According to literature finding [38,39], NLC provided a 10% of drug release at T0 suggesting the presence of a drug-rich region on the surfactants layer [40]. All formulations were able to provide a slow and prolonged release for 24 h.

The obtained release profiles resulted in agreements with previous findings on similar NLC systems developed by our research group [19], which provided a sustained and prolonged release of ferulic acid until 48 h from the beginning of the experiment. This behaviour also reflects other literature findings demonstrating that nanoparticles with diameters lower than 200 nm generally provide a burst release followed by a gradual release, while smaller ones usually provide a sustained release [38,39]. Furthermore, it was also reported that the release of the drug from the matrix is related to surfactant/lipid ratio, since increasing surfactant amounts caused a higher encapsulation of drug but also a decrease in its release rate [41]. The relation between higher encapsulation efficiency and lower release could justify (*M*)-NLC behaviour. Because of its low release, (*M*)-NLC was not further investigated.

In order to assess the potential application of NLC for ocular delivery, mucoadhesive evaluation was considered, since one of the main limitations of ophthalmic formulations is the low drug residence time on ocular surface that impairs its bioavailability. After topical instillation, the first and outermost barrier of the eye is the tear film on the ocular surface, which contains mucin, high-molecular weight glycoproteins with a protein backbone and a high carbohydrate content that contribute to the ocular mucus layer [42]. The mucus component of the tear film is currently explored as a target for drug delivery systems to

deliver drugs topically to the anterior and posterior eye segments. Taking into account these considerations, we evaluated the potential interaction of NLC suspensions with mucin in STF after incubation at physiological temperature.

As showed in Fig. 6, turbidimetric assay revealed the adsorption of mucin on NLC particles surface (NLC-muc, (*R*)-NLC-muc and (*S*)-NLC-muc), which was detected as an increase of UV absorbance compared to that of the native glycoprotein at all time point considered. The significant increase of UV absorbance is the result of aggregation processes [43] that suggests the occurrence of interactions phenomena between each particles suspension and the glycoprotein in STF.

These findings were furtherly confirmed by mucin particle method assay. As showed in Fig. 7, all samples suffered a significant variation in particles size and zeta potential after incubation with mucin confirming the occurrence of interactions [14]. The entity of interaction seems to be more evident starting from 2 h of incubation ((Fig. 7-A) and no difference can be detected among NLC samples (Fig. 7), suggesting that the mucoadhesion has to be attributed to the carrier itself and does not depends on the encapsulated drug; this result suggests that the presence of the drug being conveyed into the particles did not affect the interaction of the system with mucin. All samples maintained their homogeneity even in the presence of mucin, as revealed by PDI values ≤ 0.3 at all time points (data not reported).

Interaction occurring at mucin/formulation interface is a complex process that involves different mechanisms, such as that proposed by the wetting; electronic; adsorption; fracture; mechanical; and diffusion interlocking theories [44]. Here, the interaction was probably the result of hydrogen bonds and van der Waals interaction due to the adsorption mechanism or due to the diffusion mechanism which is governed by time and concentration gradient. Following diffusion, sufficient interpenetration depth and chain entanglements induce semi-permanent mucoadhesive bond formation [45]. However, mucoadhesion is based on the contact between the instilled formulation at the mucous surface, and the interpenetration into the mucosal layer that consolidate the formed interfacial interactions. This second phase known as "consolidation stage" is crucial for formulations undergoing higher physical stresses, such as ocular administration, since it assures the entity of their binding [46].

3.3. *In vitro cell studies*

Pharmacological effects of (*R*)-NLC and (*S*)-NLC were examined in human UM 92-1 cells by crystal violet staining.

First, non-specific cytotoxicity by NLC was checked, demonstrating that unloaded NLC does not cause overt toxicity to UM cells below 5 μM concentrations (Fig. 8-A). Then, dose-response curves were carried out to investigate antiproliferative actions by loaded or unloaded NLC and free bioactive compounds (Fig. 8-B,C). Compared to the respective blank NLC or free compound, both (*R*)-NLC (Fig. 8-B) and (*S*)-NLC (Fig. 8-C) induced a shift to the left of antiproliferative curves in UM 92-1 cells, indicating potentiation of (*R*)-(+)-MRJF22 and (*S*)-(−)-MRJF22 anticancer effects by NLC with significant extents starting at submicromolar concentrations.

Accordingly, prodrug-loaded NLC significantly inhibited UM cell proliferation at concentrations as low as 0.3 μM for (*S*)-NLC or 0.8 μM for (*R*)-NLC, compared to the vehicle control (Table 3). In contrast, blank NLC or each bioactive compound alone exerted significant antiproliferation only at $\geq$3 μM ranges (Table 3).

Moreover, estimations of inhibitory concentrations inducing 50% anticancer effects (IC_{50}) confirmed that compounds delivered to cells with NLC exhibited significantly superior antiproliferative potencies than corresponding free drugs or unloaded nanocarriers, with a ~3- or 4-fold increased anticancer activity for (*R*)-NLC and (*S*)-NLC, respectively (Table 4).

Finally, compared to (*R*)-NLC, the nanoformulation (*S*)-NLC exhibited higher antiproliferative potency (Fig. 8 and Table 4), despite less favorable drug encapsulation efficiency (Table 1) and release dynamics (Fig. 5-B). In contrast, the free prodrugs were almost identical in inhibiting UM cell proliferation (Table 4), confirming previous findings [9]. Since (*S*)-NLC particles exhibit smaller diameter sizes than (*R*)-NLC (Table 1), it could be possible that (*S*)-NLC nanocarrier dimensions provide superior cell permeation capabilities [29], associated with enhanced drug concentrations at pharmacological sites of action.

Collectively, the presented data indicate that the proposed nanostructured lipid carrier systems represent molecular facilitator tools for (*R*)-(+)-MRJF22 and (*S*)-(−)-MRJF22 anticancer pharmacology in UM 92-1 cells, probably reflecting an enhanced compound passage across cell plasma membranes and drug delivery to intracellular targets. It was already demonstrated the higher potency of (*S*)-(−)-MRJF22 – compared to racemic mixture and (*R*)-enantiomer – in reducing cell proliferation on UM 92-1 cells [9], probably related to the inhibition of HDAC, and this activity could be additive to the intrinsic antiproliferative property of the NLC itself, resulting in a potential dual function-dual target platform as a novel therapeutic strategy for UM patients [9]. In particular, dual function, dual target (*S*)-(−)-MRJF22 loaded into NLC might provide a novel therapeutic strategy for UM patients with optimal antitumor activity.

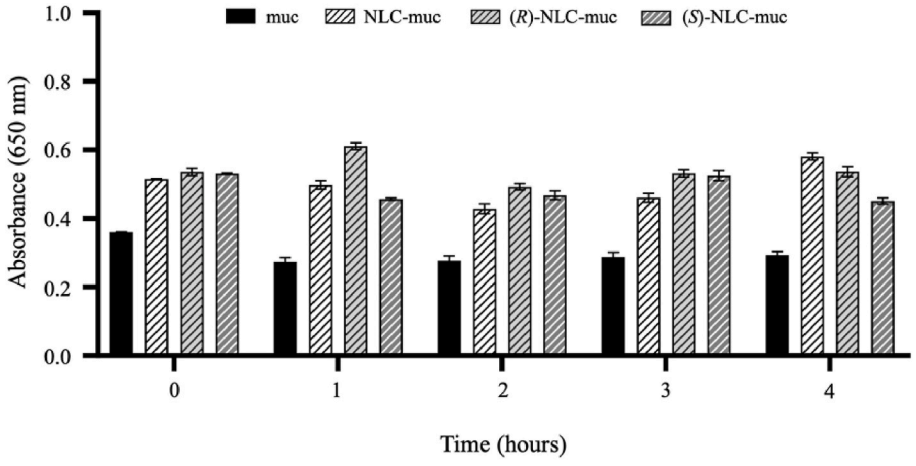

Fig. 6. *In vitro* assessment of samples/mucin interactions at different time points (0, 1, 2, 3 and 4 h) by turbidimetric assay at 650 nm. Significance was set as ****p $\leq$ 0.0001 for all samples vs mucin.

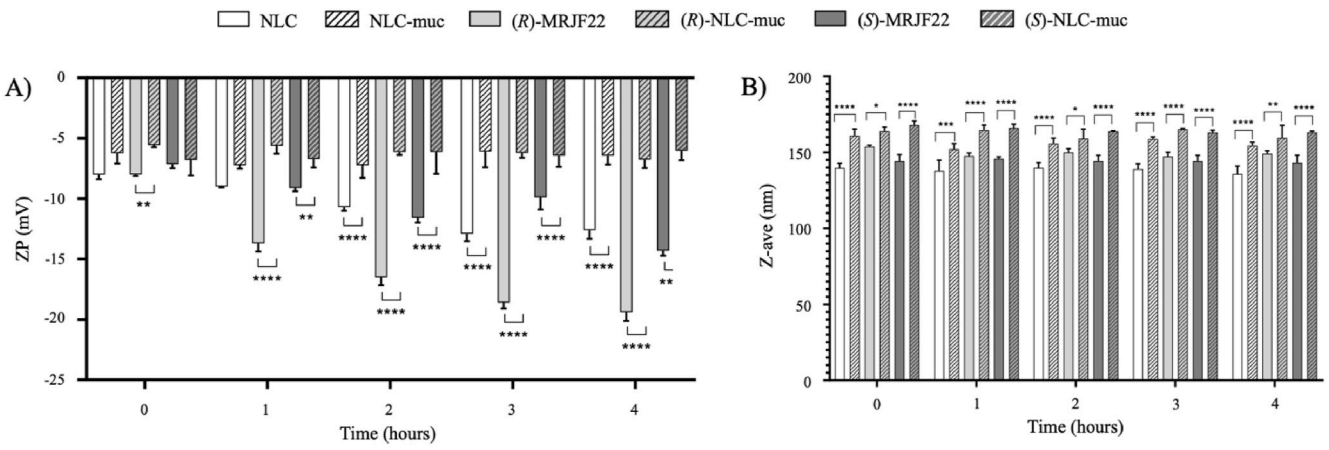

Fig. 7. Zeta potential (ZP) values (**A**) and mean particle size (Z-ave) values (**B**) of samples (NLC, (*R*)-NLC and (*S*)-NLC) before 0 and after 1, 2, 3 and 4h of incubation with mucin (NLC-muc, (*R*)-NLC-muc and (S)-NLC-muc) at 37 °C. Significance was set as **p ≤ 0.01; ****p ≤ 0.0001 for ZP; and as * p ≤ 0.05; **p ≤ 0.01; ***p ≤ 0.001; ****p ≤ 0.0001 for Z-ave.

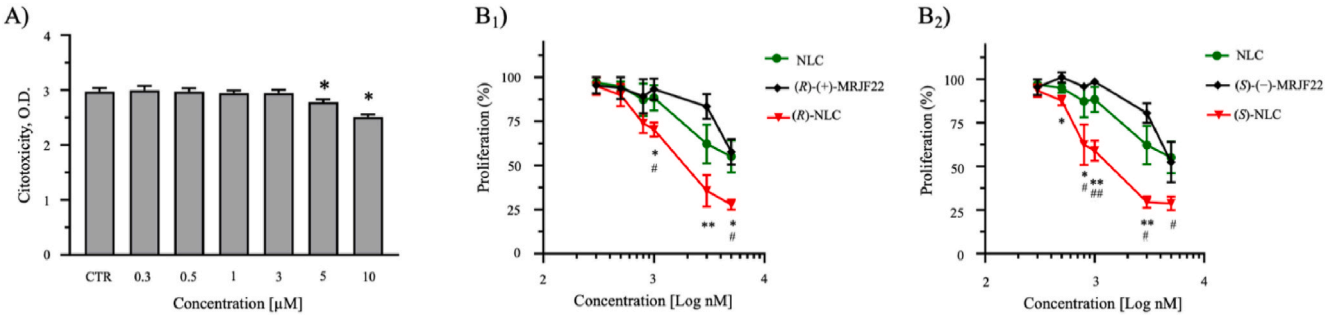

Fig. 8. Effects of anticancer prodrug-loaded NLC on UM cells. (**A**) Cytotoxicity in human 92-1 UM cells after 24 h treatment with unloaded NLC. *p < 0.05 vs CTR by unpaired Student's t-test. (**B-C**) Dose-response curves of inhibition of proliferation by the indicated compounds. Data represent % of proliferation compared to the vehicle control (DMSO). *p < 0.05; **p < 0.01 vs (*R*)-(+)-MRJF22 or (*S*)-(−)-MRJF22; #p < 0.5; ##p < 0.01 vs NLC by unpaired Student's t-test. CTR, vehicle control DMSO.

Table 3
Statistical analysis of effects on UM cell proliferation by the indicate compounds. *p < 0.05; **p < 0.01; ***p < 0.001 vs the vehicle control DMSO by unpaired Student's t-test; ns, not significant.

Dose (μM)	NLC	(*R*)-(+)-MRJF22	(*R*)-NLC	(*S*)-(−)-MRJF22	(*S*)-NLC
0.1	ns	ns	ns	Ns	Ns
0.3	ns	ns	ns	Ns	**
0.8	ns	ns	**	ns	**
1	ns	ns	***	ns	***
3	*	*	***	**	***
5	**	**	***	**	***

Table 4
IC_{50} of NLC, (*R*)-NLC, (*S*)-NLC, (*R*)-(+)-MRJF22 and (*S*)-(−)-MRJF22 on UM 92-1 cell proliferation. Data are expressed as mean ± SD. *p < 0.01 vs (*R*)-(+)-MRJF22; $ p < 0.5 vs NLC, and #p < 0.001 vs (*S*)-(−)-MRJF22 by one-tailed, unpaired Student's t-test.

Sample	IC_{50} (μM)
NLC	6.96 ± 2.96
(*R*)-NLC	2.29 ± 0.69*, $
(*S*)-NLC	1.57 ± 0.22#, $
(*R*)-(+)-MRJF22	6.45 ± 2.77
(*S*)-(−)-MRJF22	6.72 ± 0.53

4. Conclusions

The new synthetized prodrugs – both in form of racemic mixture and single enantiomers – were successfully encapsulated into lipid nanoparticles with adequate features for the intended ocular administration. Moreover, (*S*)-enantiomer loaded-NLC showed a higher *in vitro* antiproliferative activity, thus representing a safe and potentially efficient platform to be used as adjuvant in the treatment of uveal melanoma. Further studies are still ongoing to assess the NLC behavior after *in vivo* ocular administration.

Author contributions

Cinzia Cimino: conceptualization, data curation, formal analysis, investigation, methodology, writing – original draft, writing – review and editing. **Claudia Giovanna Leotta**: investigation, formal analysis, data curation, writing – original draft. **Agostino Marrazzo**: data curation, writing – review and editing, project administration. **Teresa Musumeci**: investigation, data curation, writing – original draft. **Giovanni Mario Pitari**: investigation, data curation, writing – original draft. **Rosario Pignatello**: data curation, writing – original draft, writing – review and editing. **Angela Bonaccorso**: investigation, formal analysis, data curation, writing – original draft. **Carla Barbaraci**: data curation, writing – review and editing. **Claudia Carbone**: conceptualization, funding acquisition, methodology, supervision, writing – original draft, writing – review and editing.

All authors have read and agreed to the published version of the

manuscript.

Funding

Cinzia Cimino was supported by the PhD program in Biotechnology, XXXVI cycle, University of Catania.

Institutional review board statement

Not applicable.

Informed consent statement

Not applicable.

Declaration of competing interest

The authors declare that they have no known competing financial interests or personal relationships that could have appeared to influence the work reported in this paper.

Data availability

The data that has been used is confidential.

Acknowledgments

The authors are grateful to NANOMED, Research Centre for Nanomedicine and Pharmaceutical Nanotechnology from the University of Catania for the technical assistance.

Appendix A. Supplementary data

Supplementary data to this article can be found online at https://doi.org/10.1016/j.jddst.2023.104811.

References

[1] S. Kaliki, C.L. Shields, A. Mashayekhi, A. Ganesh, M. Furuta, J.A. Shields, Influence of age on prognosis of young patients with uveal melanoma: a matched retrospective cohort study, Eur. J. Ophthalmol. 23 (2) (Mar. 2013) 208–216, https://doi.org/10.5301/ejo.5000200.

[2] F. Spagnolo, G. Caltabiano, P. Queirolo, Uveal melanoma, Cancer Treat Rev. 38 (5) (Aug. 2012) 549–553, https://doi.org/10.1016/j.ctrv.2012.01.002.

[3] A. Schmidt-Pokrzywniak, K.-H. Jöckel, N. Bornfeld, W. Sauerwein, A. Stang, Positive interaction between light Iris color and ultraviolet radiation in relation to the risk of uveal melanoma, Ophthalmology 116 (2) (Feb. 2009) 340–348, https://doi.org/10.1016/j.ophtha.2008.09.040.

[4] C.L. Shields, et al., Association of ocular and oculodermal melanocytosis with the rate of uveal melanoma metastasis: analysis of 7872 consecutive eyes, JAMA Ophthalmol 131 (8) (Aug. 2013) 993, https://doi.org/10.1001/jamaophthalmol.2013.129.

[5] Assessment of metastatic disease status at death in 435 patients with large choroidal melanoma in the collaborative ocular melanoma study (COMS), Arch. Ophthalmol. 119 (2001) 670–676.

[6] M.M. Moschos, et al., The role of histone deacetylase inhibitors in uveal melanoma: current evidence, Anticancer Res. 38 (7) (Jul. 2018) 3817–3824, https://doi.org/10.21873/anticanres.12665.

[7] S. Landreville, et al., Histone deacetylase inhibitors induce growth arrest and differentiation in uveal melanoma, Clin. Cancer Res. 18 (2) (Jan. 2012) 408–416, https://doi.org/10.1158/1078-0432.CCR-11-0946.

[8] M. Olivieri, et al., Antiangiogenic effect of (±)-Haloperidol metabolite II valproate ester [(±)-MRJF22] in human microvascular retinal endothelial cells, J. Med. Chem. 59 (21) (Nov. 2016) 9960–9966, https://doi.org/10.1021/acs.jmedchem.6b01039.

[9] C. Barbaraci, et al., Haloperidol metabolite II valproate ester (*S*)-(−)-MRJF22: preliminary studies as a potential multifunctional agent against uveal melanoma, J. Med. Chem. 64 (18) (Sep. 2021) 13622–13632, https://doi.org/10.1021/acs.jmedchem.1c00995.

[10] X.-Y. Xie, et al., Synthesis, binding, and functional properties of tetrahydroisoquinolino-2-alkyl phenones as selective σ2R/TMEM97 ligands, Eur. J. Med. Chem. 209 (Jan. 2021), 112906, https://doi.org/10.1016/j.ejmech.2020.112906.

[11] E.B. Souto, et al., Advanced formulation approaches for ocular drug delivery: state-of-the-art and recent patents, Pharmaceutics 11 (9) (Sep. 2019) 460, https://doi.org/10.3390/pharmaceutics11090460.

[12] R. Liu, Z. Liu, C. Zhang, B. Zhang, Nanostructured lipid carriers as novel ophthalmic delivery system for mangiferin: improving in vivo ocular bioavailability, J. Pharmaceut. Sci. 101 (10) (Oct. 2012) 3833–3844, https://doi.org/10.1002/jps.23251.

[13] E. Sánchez-López, M. Espina, S. Doktorovova, E.B. Souto, M.L. García, Lipid nanoparticles (SLN, NLC): overcoming the anatomical and physiological barriers of the eye – Part I – barriers and determining factors in ocular delivery, Eur. J. Pharm. Biopharm. 110 (Jan. 2017) 70–75, https://doi.org/10.1016/j.ejpb.2016.10.009.

[14] A. Bonaccorso, et al., Sorafenib repurposing for ophthalmic delivery by lipid nanoparticles: a preliminary study, Pharmaceutics 13 (11) (Nov. 2021) 1956, https://doi.org/10.3390/pharmaceutics13111956.

[15] C. Carbone, A. Campisi, T. Musumeci, G. Raciti, R. Bonfanti, G. Puglisi, FA-loaded lipid drug delivery systems: preparation, characterization and biological studies, Eur. J. Pharmaceut. Sci. 52 (Feb. 2014) 12–20, https://doi.org/10.1016/j.ejps.2013.10.003.

[16] C. Carbone, C. Caddeo, M.A. Grimaudo, D.E. Manno, A. Serra, T. Musumeci, Ferulic acid-NLC with lavandula essential oil: a possible strategy for wound-healing? Nanomaterials 10 (5) (May 2020) 898, https://doi.org/10.3390/nano10050898.

[17] D.F. Bánhegyi, D. Szolcsányi, J. Madarász, E. Pálovics, Enantiomeric separation of racemic amlodipine by sequential fractional crystallization through formation of diastereomeric salt solvates and co-crystals of solvate-like compounds with specific structure — a tandem resolution, Chirality 34 (2) (Feb. 2022) 374–395, https://doi.org/10.1002/chir.23373.

[18] L. Rizzo, S. Meric, D. Kassinos, M. Guida, F. Russo, V. Belgiorno, Degradation of diclofenac by TiO2 photocatalysis: UV absorbance kinetics and process evaluation through a set of toxicity bioassays, Water Res. 43 (4) (Mar. 2009) 979–988, https://doi.org/10.1016/j.watres.2008.11.040.

[19] C. Carbone, et al., Dual-drugs delivery in solid lipid nanoparticles for the treatment of Candida albicans mycosis, Colloids Surf. B Biointerfaces 186 (Feb. 2020), 110705, https://doi.org/10.1016/j.colsurfb.2019.110705.

[20] I. Chauhan, M. Yasir, M. Verma, A.P. Singh, Nanostructured lipid carriers: a groundbreaking approach for transdermal drug delivery, Adv. Pharm. Bull. 10 (2) (Feb. 2020) 150–165, https://doi.org/10.34172/apb.2020.021.

[21] J.-Y. Lai, Biocompatibility of chemically cross-linked gelatin hydrogels for ophthalmic use, J. Mater. Sci. Mater. Med. 21 (6) (Jun. 2010) 1899–1911, https://doi.org/10.1007/s10856-010-4035-3.

[22] C. Carbone, et al., Mediterranean essential oils as precious matrix components and active ingredients of lipid nanoparticles, Int. J. Pharm. 548 (1) (Sep. 2018) 217–226, https://doi.org/10.1016/j.ijpharm.2018.06.064.

[23] L.T. Lim, E.Y. Ah-Kee, C.E. Collins, Common eye drops and their implications for pH measurements in the management of chemical eye injuries, Int. J. Ophthalmol. 7 (6) (2014) 1067–1068, https://doi.org/10.3980/j.issn.2222-3959.2014.06.29.

[24] W.H. Coles, P.A. Jaros, Dynamics of ocular surface pH, Br. J. Ophthalmol. 68 (8) (Aug. 1984) 549–552, https://doi.org/10.1136/bjo.68.8.549.

[25] R. Pignatello, Optimization and validation of a new method for the production of lipid nanoparticles for ophthalmic application, Int. J. Med. Nano Res. 1 (1) (Dec. 2014), https://doi.org/10.23937/2378-3664/1410006.

[26] A. Tatke, et al., In situ gel of triamcinolone acetonide-loaded solid lipid nanoparticles for improved topical ocular delivery: tear kinetics and ocular disposition studies, Nanomaterials 9 (1) (Dec. 2018) 33, https://doi.org/10.3390/nano9010033.

[27] M. Yadav, et al., Atorvastatin-loaded solid lipid nanoparticles as eye drops: proposed treatment option for age-related macular degeneration (AMD), Drug Deliv. Transl. Res. 10 (4) (Aug. 2020) 919–944, https://doi.org/10.1007/s13346-020-00733-4.

[28] A.L. Onugwu, A.A. Attama, P.O. Nnamani, S.O. Onugwu, E.B. Onuigbo, V. V. Khutoryanskiy, Development and optimization of solid lipid nanoparticles coated with chitosan and poly(2-ethyl-2-oxazoline) for ocular drug delivery of ciprofloxacin, J. Drug Deliv. Sci. Technol. 74 (Aug. 2022), 103527, https://doi.org/10.1016/j.jddst.2022.103527.

[29] L. Bonilla, et al., Lipid nanoparticles for the posterior eye segment, Pharmaceutics 14 (1) (Dec. 2021) 90, https://doi.org/10.3390/pharmaceutics14010090.

[30] H. Rouco, et al., Rifabutin-loaded nanostructured lipid carriers as a tool in oral anti-mycobacterial treatment of crohn's disease, Nanomaterials 10 (11) (Oct. 2020) 2138, https://doi.org/10.3390/nano10112138.

[31] G.I. Sakellari, I. Zafeiri, H. Batchelor, F. Spyropoulos, Formulation design, production and characterisation of solid lipid nanoparticles (SLN) and nanostructured lipid carriers (NLC) for the encapsulation of a model hydrophobic active, Food Hydrocoll. Health 1 (2021), 100024, https://doi.org/10.1016/j.fhfh.2021.100024.

[32] W. Mehnert, Solid lipid nanoparticles Production, characterization and applications, Adv. Drug Deliv. Rev. 47 (2–3) (Apr. 2001) 165–196, https://doi.org/10.1016/S0169-409X(01)00105-3.

[33] M. Agrawal, et al., Design and optimization of curcumin loaded nano lipid carrier system using Box-Behnken design, Biomed. Pharmacother. 141 (Sep. 2021), 111919, https://doi.org/10.1016/j.biopha.2021.111919.

[34] U. Ilyas, et al., Nanostructured lipid carrier-based delivery of pioglitazone for treatment of type 2 diabetes, Front. Pharmacol. 13 (Jul. 2022), 934156, https://doi.org/10.3389/fphar.2022.934156.

[35] E. Zingale, et al., Optimization of lipid nanoparticles by response surface methodology to improve the ocular delivery of diosmin: characterization and in-vitro anti-inflammatory assessment, Pharmaceutics 14 (9) (Sep. 2022) 1961, https://doi.org/10.3390/pharmaceutics14091961.

[36] V. Teeranachaideekul, B. Morakul, P. Boonme, W. Pornputtapitak, V. Junyaprasert, Effect of lipid and oil compositions on physicochemical properties and photoprotection of octyl methoxycinnamate-loaded nanostructured lipid carriers (NLC), J. Oleo Sci. 69 (12) (2020) 1627–1639, https://doi.org/10.5650/jos.ess20093.

[37] P. Chand, et al., Design and evaluation of cabazitaxel loaded NLCs against breast cancer cell lines, Colloids Surf. B Biointerfaces 199 (Mar. 2021), 111535, https://doi.org/10.1016/j.colsurfb.2020.111535.

[38] E. Sakurai, H. Ozeki, N. Kunou, Y. Ogura, Effect of particle size of polymeric nanospheres on intravitreal kinetics, Ophthalmic Res. 33 (1) (2001) 31–36, https://doi.org/10.1159/000055638.

[39] Y. Weng, J. Liu, S. Jin, W. Guo, X. Liang, Z. Hu, Nanotechnology-based strategies for treatment of ocular disease, Acta Pharm. Sin. B 7 (3) (May 2017) 281–291, https://doi.org/10.1016/j.apsb.2016.09.001.

[40] P.A. Makoni, K. Wa Kasongo, R.B. Walker, Short term stability testing of efavirenz-loaded solid lipid nanoparticle (SLN) and nanostructured lipid carrier (NLC) dispersions, Pharmaceutics 11 (8) (Aug. 2019) 397, https://doi.org/10.3390/pharmaceutics11080397.

[41] B. Sharif Makhmal Zadeh, H. Niro, F. Rahim, G. Esfahani, Ocular delivery system for propranolol hydrochloride based on nanostructured lipid carrier, Sci. Pharm. 86 (2) (Apr. 2018) 16, https://doi.org/10.3390/scipharm86020016.

[42] G. As Georgiev, P. Eftimov, N. Yokoi, Contribution of mucins towards the physical properties of the tear film: a modern update, Int. J. Mol. Sci. 20 (24) (Dec. 2019) 6132, https://doi.org/10.3390/ijms20246132.

[43] P.N. Hanieh, et al., Almond oil O/W nanoemulsions: potential application for ocular delivery, J. Drug Deliv. Sci. Technol. 72 (Jun. 2022), 103424, https://doi.org/10.1016/j.jddst.2022.103424.

[44] S. Duggan, W. Cummins, O. O' Donovan, H. Hughes, E. Owens, Thiolated polymers as mucoadhesive drug delivery systems, Eur. J. Pharmaceut. Sci. 100 (Mar. 2017) 64–78, https://doi.org/10.1016/j.ejps.2017.01.008.

[45] A.M. Burhan, et al., Posterior segment ophthalmic drug delivery: role of muco-adhesion with a special focus on chitosan, Pharmaceutics 13 (10) (Oct. 2021) 1685, https://doi.org/10.3390/pharmaceutics13101685.

[46] J. Smart, The basics and underlying mechanisms of mucoadhesion, Adv. Drug Deliv. Rev. 57 (11) (Nov. 2005) 1556–1568, https://doi.org/10.1016/j.addr.2005.07.001.